Isolation of Lymphocytes from Human Skin and Murine Tissues: A Rapid and Epitope-Preserving Approach

Alexandra Polakova[1], Christoph Hudemann[1], Felix Wiemers[2], Arturas Kadys[2], Niklas Gremke[2], Manuel Lang[3], Lutz Zwiorek[2], Wolfgang Pfützner[1], Michael Hertl[1], Christian Möbs[1] and Christine L. Zimmer[1]

Tissue-resident immune cells have been shown to play an important role in skin health and disease. However, owing to limited access to human skin samples and time-consuming, technically demanding protocols, the characterization of tissue-derived cells remains challenging. For this reason, blood-derived leukocytes are frequently used as a surrogate specimen, although they do not necessarily reflect local immune responses in the skin. Therefore, we aimed to establish a rapid protocol to isolate a sufficient number of viable immune cells from 4-mm skin biopsies that can be directly used for a deeper characterization such as comprehensive phenotyping and functional studies of T cells. In this optimized protocol, only two enzymes, type IV collagenase and DNase I, were used to achieve both the highest possible cellular yield and marker preservation of leukocytes stained for multicolor flow cytometry. We further report that the optimized protocol may be used in the same manner for murine skin and mucosa. In summary, this study allows a rapid acquisition of lymphocytes from human or mouse skin suitable for comprehensive analysis of lymphocyte subpopulations, for disease surveillance, and for identification of potential therapeutic targets or other downstream applications.

JID Innovations (2023);**3:**100155 doi:10.1016/j.xjidi.2022.100155

INTRODUCTION

Studies published over the past decade have increasingly shed light on the importance of innate and adaptive tissue-resident immune cells in health and disease (Ho and Kupper, 2019; Szabo et al., 2019). However, owing to its accessibility, blood remains a major source of research material for human immune cell studies even though blood-derived leukocytes do not necessarily reflect local immune responses in the skin. Hence, skin-derived leukocytes are crucial to elucidate pathophysiological processes in skin diseases (Szabo et al., 2019). It is estimated that healthy human skin contains about 20 billion αβ T cells, some macrophages, dendritic cells, and to a lesser extent, NK cells, γδ T cells, and innate lymphoid cells (ILCs) (Ho and Kupper, 2019; Watanabe et al., 2015). This composition may change in inflammatory skin diseases, such as psoriasis, atopic dermatitis, pemphigus, or pemphigoid, which are characterized by a mixed cutaneous immune cell infiltrate (Egami et al., 2020; Ho and Kupper, 2019; Watanabe et al., 2015).

Tissue-resident memory T (T_{RM}) cells have been shown to permanently reside in various tissues, including the gut, liver, lung, and skin (Oja et al., 2018; Pallett et al., 2020; Sathaliyawala et al., 2013; Strobl et al., 2020; Watanabe et al., 2015; Wong et al., 2016). They can be distinguished from their circulating counterparts by the expression of tissue-residency markers, such as CD69, CD49a, and CD103 (Kumar et al., 2017; Szabo et al., 2019; Watanabe et al., 2015). T_{RM} cells have been characterized and shown to play a role in various cutaneous diseases, such as psoriasis, atopic dermatitis, alopecia areata, vitiligo, graft-versus-host disease, and pemphigus vulgaris (Cheuk et al., 2017; Ho and Kupper, 2019; Park and Kupper, 2015; Strobl et al., 2020; Zou et al., 2021). Moreover, recent technological advances have opened the field for a detailed characterization of other rare immune cell subsets, such as ILCs (Alkon et al., 2022; Simoni et al., 2017).

Owing to limited access to human skin samples and time-consuming, technically demanding protocols, the characterization of these cells remains challenging. Therefore, the isolation of immune cells using a protocol optimized for a particular tissue is of great importance, ensuring optimal cell viability, cellular yield, and epitope preservation for adequate phenotyping. Previous studies have used various approaches, such as tissue explants, EDTA isolation, or enzymatic digestion (Brüggen et al., 2014; Cheuk et al., 2014; Clark et al., 2006b; Salimi et al., 2016; Sanchez Rodriguez et al., 2014; Sato et al., 2022; Zou et al., 2021). However, these methods either require long incubation times, a combination of many

[1]*Department of Dermatology and Allergology, Philipps-Universität Marburg, Marburg, Germany;* [2]*Department of Gynecology and Obstetrics, Philipps-Universität Marburg, Marburg, Germany; and* [3]*Center for Human Genetics, Philipps-Universität Marburg, Marburg, Germany*

Correspondence: Christine L. Zimmer, Department of Dermatology and Allergology, Philipps-Universität Marburg, Baldingerstraße, Marburg 35043, Germany. E-mail: christine.zimmer@uni-marburg.de

Abbreviations: ILC, innate lymphoid cell; T_{EM}, effector memory T; T_{RM}, tissue-resident memory T; UMAP, unsupervised uniform manifold approximation and projection analysis

Received 15 December 2021; revised 30 June 2022; accepted 5 July 2022; accepted manuscript published online 7 September 2022; corrected proof published online 9 December 2022

Cite this article as: JID Innovations 2023;3:100155

Table 1. Participants Characteristics

		Individuals
Group Size	**n**	**34**
Demographics	Age, median (range)	57 (18–91)
	Male sex, n (%)	4 (12)
	Female sex, n (%)	30 (88)
Location (origin of skin)	Breast, n (%)	32 (94)
	Forehead, n (%)	1 (3)
	Cheek, n (%)	1 (3)

different enzymes, or even immune cell tissue egress over several days. The lack of a rapid, optimized protocol for the isolation of immune cells from small skin biopsies, routinely taken for diagnostic purposes in the clinic, prompted us to develop a sophisticated and at the same time user-friendly method. We aimed to establish a protocol that allowed for both immediate processing of the samples from clinical practice and simple handling without the need for expensive technical equipment or complicated labor-intensive procedures.

Using an enzymatic digestion protocol, an average of 12,000 live $CD45^+$ lymphocytes was obtained after mechanical digestion of 4-mm skin biopsy specimens with optimized concentrations of only two enzymes, type IV collagenase and DNase. These were subsequently subjected to multicolor flow cytometry. Our protocol has proved to be suitable for isolating various lymphocyte subsets after a 30-minute period of digestion while preserving epitope expression. Thus, it can be utilized for a detailed phenotypic characterization of T cells, including chemokine receptors that are prone to be affected by longer digestion periods. Moreover, isolated T cells retain their functional capacity on polyclonal stimulation with phorbol 12-myristate-13-acetate/ionomycin. We further report that our rapid isolation protocol can be used in the same manner for murine skin and mucosa. Together, we present a sophisticated yet simple and time-saving method to isolate live immune cells from small skin biopsies, which can be used for several downstream applications, including flow cytometry, cell culture, or RNA sequencing.

RESULTS

Optimized protocol preserves the expression of cell surface markers while enabling high cell yield

Punch biopsies in a size of 4 mm are routinely taken for diagnostic purposes in the clinic. Considering the limited material, a rapid and simple protocol for the isolation of immune cells would be of great advantage. This prompted us to develop, to our knowledge, a previously unreported approach to address these needs. For this purpose, skin biopsies and peripheral blood samples were collected from 34 individuals during elective surgical procedures, mainly breast reduction surgeries. A detailed description of the cohort is shown in Table 1.

To isolate immune cells, skin biopsies were minced and subjected to an enzymatic digestion with collagenase IV and DNase I for different time periods on a magnetic stirrer at 37 °C. Subsequently, the skin fragments were filtered, pelleted, and analyzed using high-dimensional flow cytometry (Figures 1 and 2a). The detailed protocol and a corresponding graphical description can be found in the Materials and Methods and Figure 1, respectively. As a starting point, experimental conditions were grounded on other tissue isolation protocols (Brüggen et al., 2014; Cheuk et al., 2017; Sanchez Rodriguez et al., 2014; Zou et al., 2021). The cellular yield was determined by gating on live $CD45^+CD14^-CD19^-$ lymphocytes and $CD3^+$ T cells (Figure 2b) on enzymatic digestion with 3 mg/ml collagenase IV at different incubation times. The highest yield of both live $CD45^+CD14^-CD19^-$ lymphocytes and $CD3^+$ T cells was obtained after 45 minutes of digestion with 3 mg/ml of collagenase IV. Because the cellular yield declined drastically on 90 minutes of digestion, shorter time points were chosen for the following experiments. Of note, using 1 mg/ml of collagenase IV resulted in comparable cellular yields at the 45-minute time point (Figure 2c). To further optimize the enzymatic concentrations, we used low and high concentrations of collagenase IV (1 and 3 mg/ml, respectively) in combination with low and high concentrations of DNase I (0.2 and 1 mg/ml, respectively). All in all, 45 minutes of digestion with 3 mg/ml of collagenase IV resulted in the highest yield (Figure 2d). However, considering epitope preservation, we observed a distinct downregulation of CD4 at all time points when 3 mg/ml of collagenase IV was used. The best preservation of the CD4 epitope was achieved at an incubation time of 30 minutes with 1 mg/ml collagenase IV and 0.2 mg/ml DNase I (Figure 2e). Next, we identified the optimal concentration of collagenase IV in terms of the cellular yield on enzymatic digestion of 30 minutes with 0.2 mg/ml DNase, which peaked at 1.7 mg/ml (Figure 2f). Moreover, the expression of the chemokine receptors CXCR3 and CCR6, which have previously been reported to play a role in skin-homing and are easily affected by enzymatic digestion (Nieto et al., 2012; Reichard and Asosingh, 2019), was shown to be preserved (Figure 2g).

For standardization purposes, punch biopsies of 4 mm were taken from larger skin samples to optimize the protocol. To further validate the protocol on other standardized punch biopsy sizes used in the clinic, 6- and 8-mm punches were additionally included for comparison. The number of cells isolated from the skin increased with the enlarging size of the skin biopsy sample (Figure 2h), whereas the percentage of the corresponding cell subsets out of live $CD45^+$ leukocytes remained consistent (Figure 2i). Therefore, the rapid isolation protocol can be used to isolate immune cells from conventional skin biopsies of 4, 6, and 8 mm in size. Of note, although the rapid protocol was optimized on rather homogeneous skin samples (i.e., breast skin), it is equally applicable to other anatomical regions such as the face, oral mucosa, back, abdomen, and upper and lower extremities (data not shown). In summary, considering cellular yield and epitope preservation, we established a protocol for isolation of immune cells from conventional biopsies with optimized concentrations of collagenase IV and DNase I and an enzymatic digestion time of 30 minutes.

Rapid isolation of innate and adaptive lymphocytes

Next, we investigated whether our protocol allows the isolation of other innate and adaptive leukocytes from human

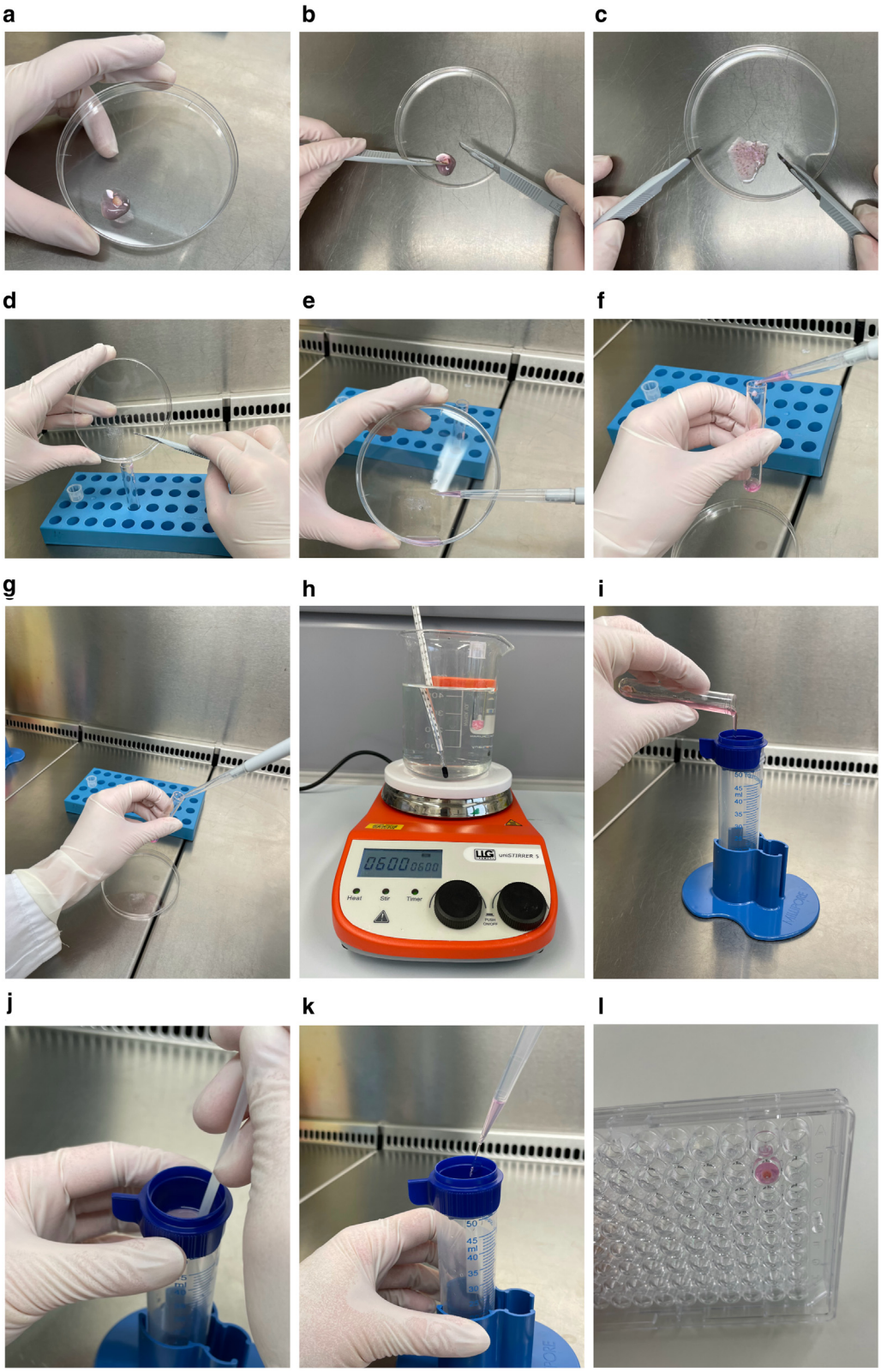

Figure 1. Photo demonstration of the skin digestion protocol. (**a**) Biopsy in incomplete RPMI 1640 medium. (**b**) Mechanical mincing of the biopsy with scalpels. (**c**) Small fragments after mechanical digestion of the skin biopsy. (**d**) Transfer of small fragments into a test tube. (**e**) Flushing of the petri dish. (**f**) Pooling of the remaining fragments and cells (final volume 500 µl). (**g**) Addition of enzymes and magnet. (**h**) Incubation of the test tube in a water bath on a magnetic stirrer using a floating rack. (**i**) Filtering the suspension through a 40-µm filter. (**j**) Pushing the final pieces of tissue through the filter with a sterile syringe plunger. (**k**) Flushing the filter with 2 ml of complete RPMI 1640 medium. (**l**) Skin pellet plated in a 96-well plate after centrifugation. DCM, dead cell marker; FSC-A, forward scatter area; FSC-H, forward scatter height; min, minute; SSC-A, side scatter area.

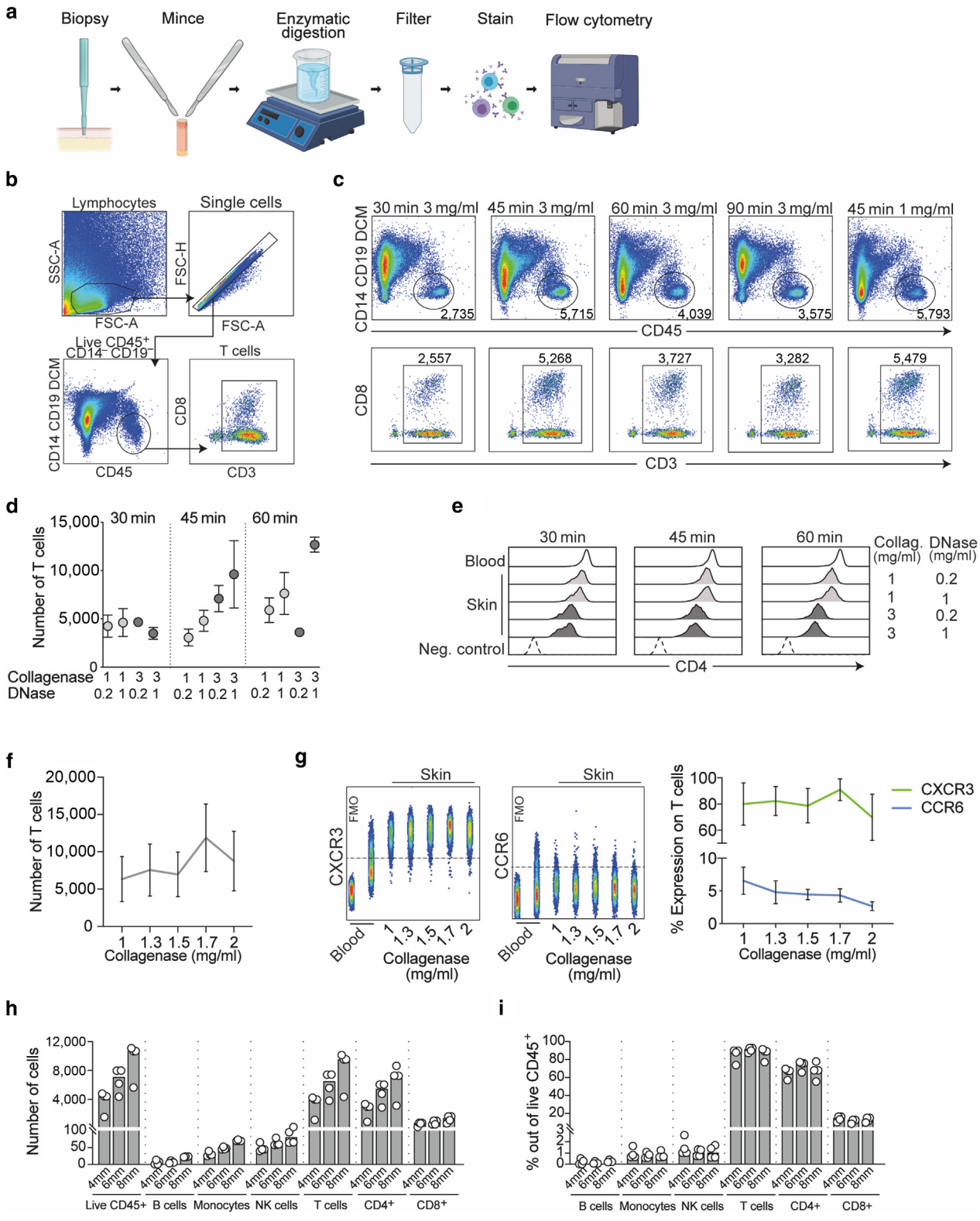

Figure 2. Establishing optimal conditions for immune cell isolation. (**a**) Workflow showing the acquisition and processing of skin biopsies. (**b**) Gating strategy to identify live $CD45^{+}CD14^{-}CD19^{-}$ lymphocytes and T cells in blood and skin. (**c**) Representative flow cytometry plots depicting live $CD45^{+}CD14^{-}CD19^{-}$ lymphocytes and total T-cell numbers after digestion with 1 mg/ml of DNase I and the respective collagenase IV concentrations for different incubation periods. (**d**) The number of T cells identified by flow cytometry in the skin during digestion under different conditions. Light gray dots represent the concentrations of 1 mg/ml, and dark gray dots represent the concentrations of 3 mg/ml collagenase IV (mean ± SEM; n = 3–5). Statistical significance was tested using Kruskal–Wallis test followed by Dunn's multiple comparisons test. (**e**) Representative histograms portraying CD4 expression and its loss under different conditions. Light gray–filled histograms show the use of 1 mg/ml, and dark gray–filled histograms show that of 3 mg/ml collagenase IV. Depicted is one representative dataset of three independent experiments. (**f**) The number of T cells identified by flow cytometry in the skin during digestion with different concentrations of collagenase IV and 0.2 mg/ml of DNase for 30 minutes (mean ± SEM; n = 3). Statistical significance was tested using Friedman test, followed by Dunn's multiple comparisons

skin biopsies. The following five major types of leukocytes were identified using flow cytometry: (i) live lymphocytes ($CD45^+CD14^-$) divided into (ii) T cells ($CD45^+CD3^+$) and (iii) B cells ($CD45^+CD3^-CD19^+$), (iv) NK cells ($CD45^+CD3^-CD56^{dim/bright}$), and (v) ILCs ($CD45^+$lineage$^-CD127^+CD161^+$) (Figure 3a). Among human skin $CD45^+CD14^-$ lymphocytes, T cells were the most abundant population, followed by NK cells, B cells, and ILCs being a rare population in terms of both number (Figure 3b) and frequency (Figure 3c). Interestingly, digestion times longer than 30 minutes showed a tendency toward higher cell yields for most populations, except for NK cells, which decreased after 45 and 90 minutes most likely owing to the loss of CD56. This change in subset distribution could also be visualized for digestion times longer than 30 minutes (Figure 3c). Moreover, the longest digestion period of 90 minutes resulted in a notable decrease in the detection of ILCs and a significant decrease in NK cell numbers, suggesting that besides an enzymatic impact on epitopes, cell death of specific immune cell populations can be induced during prolonged enzymatic digestion. Of note, differences in the distribution of immune cell subsets between peripheral blood and skin, that is, a higher abundance of $CD56^{dim}$ NK cells and B cells in the blood, could be clearly shown in terms of cell frequency by conventional gating (Figure 3c) and by unsupervised clustering (Figure 3d, upper row), respectively. To this end, we performed an unsupervised uniform manifold approximation and projection (UMAP) analysis, which visualizes multivariate relationships between phenotypic markers. On the contrary, the frequencies of ILCs and $CD56^{bright}$ NK cells among $CD45^+CD14^-$ lymphocytes were higher in human skin. Observed differences in absolute numbers of cells in skin biopsies at different digestion periods were re-evaluated using UMAP analysis (Figure 3d, lower row). To determine absolute cell counts in 4-mm skin biopsies, we made use of counting beads. In two analyzed donors, counting beads were added to the skin samples before digestion in addition to the enzymes, and absolute numbers of cells were extrapolated using total events and counting beads (Figure 3e). The results corroborated that among lymphocytes, T cells were the most prominent cell type in healthy human adult skin, followed by B cells, NK cells, and ILCs (Figure 3e). To test our protocol against a commercially available kit, 4-mm skin biopsies were simultaneously digested using our optimized rapid protocol and a commercially available procedure, including enzymatic skin dissociation and automated tissue disruption. In terms of absolute numbers, all monitored leukocyte populations isolated from the skin were comparable (Figure 3f). However, manual cell isolation proved to be gentler and thus more effective in terms of cell marker preservation (Figure 3g). Surface markers such as CD69, CD8, CXCR3, and CCR4 were readily lost using the commercially available tissue dissociation process in comparison with using the manual rapid isolation protocol.

Furthermore, in addition to lymphocytes, our rapid isolation protocol has also been shown to be effective for the isolation and identification of myeloid immune cell subsets from healthy skin (Figure 4a and b). Taken together, these results showed that the optimized protocol can be used to effectively isolate the leukocytes mentioned earlier from human skin.

Characterization of distinct T-cell subsets derived from human skin

Using the optimized protocol, we next characterized isolated T cells as the main lymphocyte subset present in the skin from biopsies and matched peripheral blood of 10 donors. Samples were processed and stained for conventional T cells, including $CD4^+$; $CD8^+$ T cells; regulatory T cells; and unconventional T cells, such as γδ T cells and mucosal-associated invariant T cells, which have been reported to be enriched among tissue-resident lymphocytes (Fan and Rudensky, 2016; Hoytema van Konijnenburg and Mucida, 2017). On the basis of the expression of nine phenotypic markers (CD103, CD69, CD49a, CD4, CD8, CD127, CD25, TCRγδ, and MR1 5-OP-RU), we performed a UMAP analysis on T cells isolated from skin and matched peripheral blood (Figure 5a). As expected, T cells isolated from skin clustered differently from T cells isolated from peripheral blood (Figure 5b, upper row). A more detailed investigation of T-cell subsets revealed that both compartments consisted of conventional T cells and regulatory T cells, whereas only a minor fraction of γδ T cells and mucosal-associated invariant T cells could be found in the skin. Nevertheless, we observed that the clusters of the same subsets mapped differently for blood from that of the skin (Figure 5b, lower row).

Given that the skin is a physical barrier tissue, we expected that a considerable fraction of immune cells would display a tissue-resident phenotype (Chen and Shen, 2020; Szabo et al., 2019). High expression of CD69, CD49a, and CD103 could be detected on skin T cells in addition to lineage markers (Figure 5a and b), with $CD69^+CD103^+$ cells being one of the most prevalent populations. To define the T-cell populations with a tissue-resident phenotype, we mapped the tissue-residency markers back onto the T-cell subsets and found that the differential clustering in the skin was due to the expression of CD69, CD49a, and CD103 (Figure 5b, lower row). The clustering revealed $CD4^+$ T cells and $CD8^+$ T cells to be the major immune cell populations expressing CD69 and CD103, with mostly $CD8^+$ T cells coexpressing CD49a. In contrast, both peripheral blood $CD4^+$ and $CD8^+$ T cells rarely expressed any of them. Thus, we found that conventional T cells were the major subsets expressing tissue-residency markers in the skin.

T cells isolated from skin retain their functional capacities

To evaluate whether T cells isolated from the human skin are functional, skin-derived T cells were polyclonally

test. (**g**) Flow cytometry plots and summary graph depicting CXCR3 and CCR6 expression on T cells during digestion with the conditions described in **f**. In the summary graph, the green line depicts the expression of CXCR3 on T cells, and the blue line depicts the expression of CCR6 on T cells (mean ± SEM; n = 3). Statistical significance was tested using Friedman test, followed by Dunn's multiple comparisons test. (**h**) The number of live $CD45^+$ leukocytes, B cells, monocytes, NK cells, T cells, $CD4^+$ T cells, and $CD8^+$ T cells and (**i**) the percentage of these cell types after applying the rapid lymphocyte isolation protocol (median; n = 4). Differences did not reach significance. DCM, dead cell marker; FSC-A, forward scatter area; FSC-H, forward scatter height; SSC-A, side scatter area; ns, not significant.

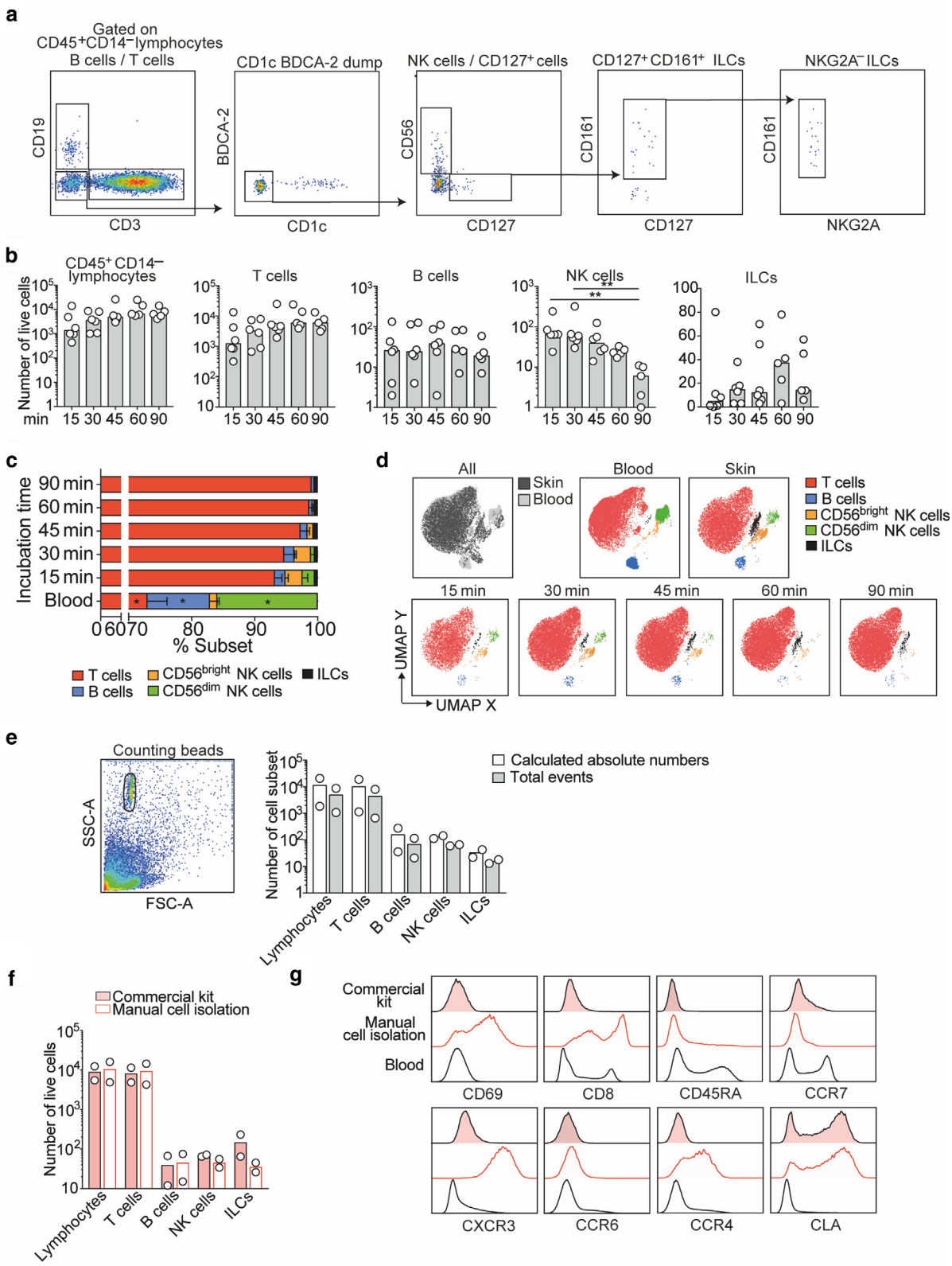

Figure 3. Detection of innate and adaptive lymphocytes in the skin during digestion at different time points. (**a**) Representative flow cytometry plots showing the gating strategy for B cells, T cells, NK cells, and ILCs. (**b**) Summary graphs depicting the absolute numbers of live cells for $CD45^{+}CD14^{-}$ lymphocytes, T cells, B cells, NK cells, and ILCs after the digestion of skin biopsies at different incubation periods (15, 30, 45, 60, and 90 minutes) with 1.7 mg/ml of collagenase and 0.2 mg/ml of DNase (median; n = 6). Statistical significance was tested using Kruska–Wallis test, followed by Dunn's multiple comparisons test. $^{**}P < 0.01$. (**c**) Relative frequency of different immune cell subsets in peripheral blood and skin biopsies at different incubation periods of digestion (mean + SEM; n = 6). Statistical significance was tested using Wilcoxon matched-pairs signed rank test. Statistical significance between blood and skin $^{*}P < 0.05$. (**d**) UMAP illustrating the differences between skin and blood and the respective immune cell populations for all cells (upper row) and for the respective incubation periods used for skin (lower row; mean, n = 6). (**e**) Representative flow cytometry plot showing the identification of counting beads in the FSC-A and SSC-A. Numbers of

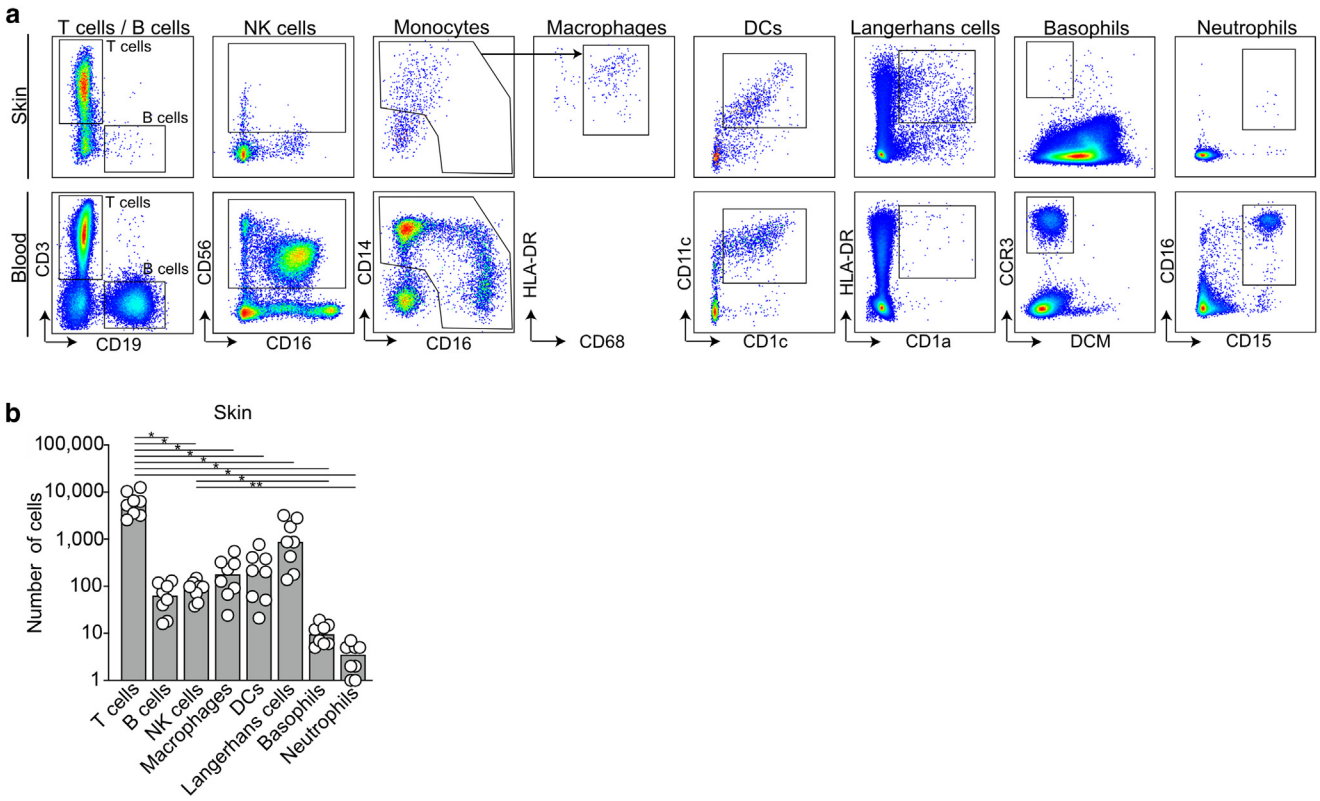

Figure 4. Detection of lymphoid and myeloid immune cells from healthy skin using the 30-minute digestion protocol. (**a**) Representative flow cytometry plots showing the gating strategy for ($CD45^+CD19^-CD3^+$) T cells, ($CD45^+CD19^+CD3^-$) B cells, ($CD45^+CD3^-CD19^-CD16^{+/-}CD56^+$) NK cells, ($CD45^+CD3^-CD19^-HLA\text{-}DR^+CD14^{+/-}CD16^{+/-}$) monocytes, ($CD45^+CD3^-CD19^-$ $HLA\text{-}DR^+CD14^{+/-}CD16^{+/-}CD68^+$) macrophages, ($CD45^+CD3^-CD19^-HLA\text{-}DR^+CD14^-CD16^{+/-}CD1c^+CD11c^+$) DCs, ($CD14^-HLA\text{-}DR^+CD1a^+$) Langerhans cells, ($CD45^-CD3^-CD19^-HLA\text{-}DR^-CD14^-CD16^-CD56^-CCR3^+$) basophils, and ($CD45^-CD3^-CD19^-CD56^-HLA\text{-}DR^-CD15^+CD16^+$) neutrophils in the skin and blood. The lack of the flow cytometry plot showing macrophages in the lower row is due to the absence of these cells in peripheral blood. Peripheral blood monocytes are a source of skin-infiltrating macrophages as shown in pathological settings (Geissmann et al., 2010; Hashimoto et al., 2013). (**b**) Summary graphs depicting the absolute numbers of live cells isolated from the skin as shown in **a** (median, n = 8). Statistical significance was tested using RM one-way ANOVA followed by Tukey's multiple comparison test. $*P < 0.05$ and $**P < 0.01$. DC, dendritic cell; RM, repeated measure.

stimulated with phorbol 12-myristate-13-acetate and ionomycin. Ex vivo, skin T cells were highly functional and produced all investigated cytokines, including IFN-γ, IL-4, IL-17, and IL-21 (Figure 6a). Cytokine profiles of T cells were assessed and compared with those of T cells from matched peripheral blood and their respective unstimulated controls. Among six samples, IFN-γ, IL-4, and IL-21 were more readily produced by peripheral T cells (Figure 6b). Nevertheless, skin T cells produced more IL-17 than their blood-derived counterparts (Figure 6b). Together, these results strongly suggest that skin-derived T cells isolated by our protocol are highly functional and can be used for further downstream applications.

Optimized protocol of rapid skin isolation can be utilized for immune cell retrieval from murine tissues

Next, we set out to validate the universal applicability of our rapid skin isolation protocol. The optimized protocol was used to digest 0.25–1 cm^2 of murine skin and murine buccal mucosa. Murine skin and mucosa samples were digested using our protocol, and blood was lysed for PBMC retrieval, followed by staining for flow cytometry. Substantial differences between murine blood and the murine tissues—skin and mucosa—could be observed (Figure 7a–c). Further analysis of cells isolated from mice revealed that both skin and mucosa contained notable absolute numbers of live $CD45^+CD14^-$ lymphocytes. $CD3^+$ T cells represented a

live $CD45^+CD14^-$ lymphocytes, T cells, B cells, NK cells, and ILCs were extrapolated using the absolute number of events and counting beads in the skin during digestion (mean, n = 2). Statistical significance was tested using Mann–Whitney test; ns. (**f**) Numbers of live $CD45^+CD14^-$ lymphocytes, T cells, B cells, NK cells, and ILCs identified by flow cytometry in the skin during the digestion of skin using either a commercially available whole-skin dissociation kit Commercial kit (black-lined bar filled with red, n = 2) or the rapid isolation protocol with collagenase IV and DNase Manual cell isolation (unfilled red-lined bar, mean, n = 2). Statistical significance was tested using Mann–Whitney test. (**g**) Representative histograms showing the expression of CD69, CD8, CD45RA, CCR7, CXCR3, CCR6, CCR4, and CLA in the blood (unfilled black line) compared with that of skin-derived T cells processed with a commercially available whole-skin dissociation kit Commercial kit (black line filled with red) and the rapid isolation protocol with collagenase and DNase Manual cell isolation (unfilled red line). Histograms depict one representative dataset of two independent experiments. Differences did not reach significance. FSC-A, forward scatter area; ILC, innate lymphoid cell; ns, not significant; SSC-A, side scatter area; UMAP, unsupervised uniform manifold approximation and projection analysis.

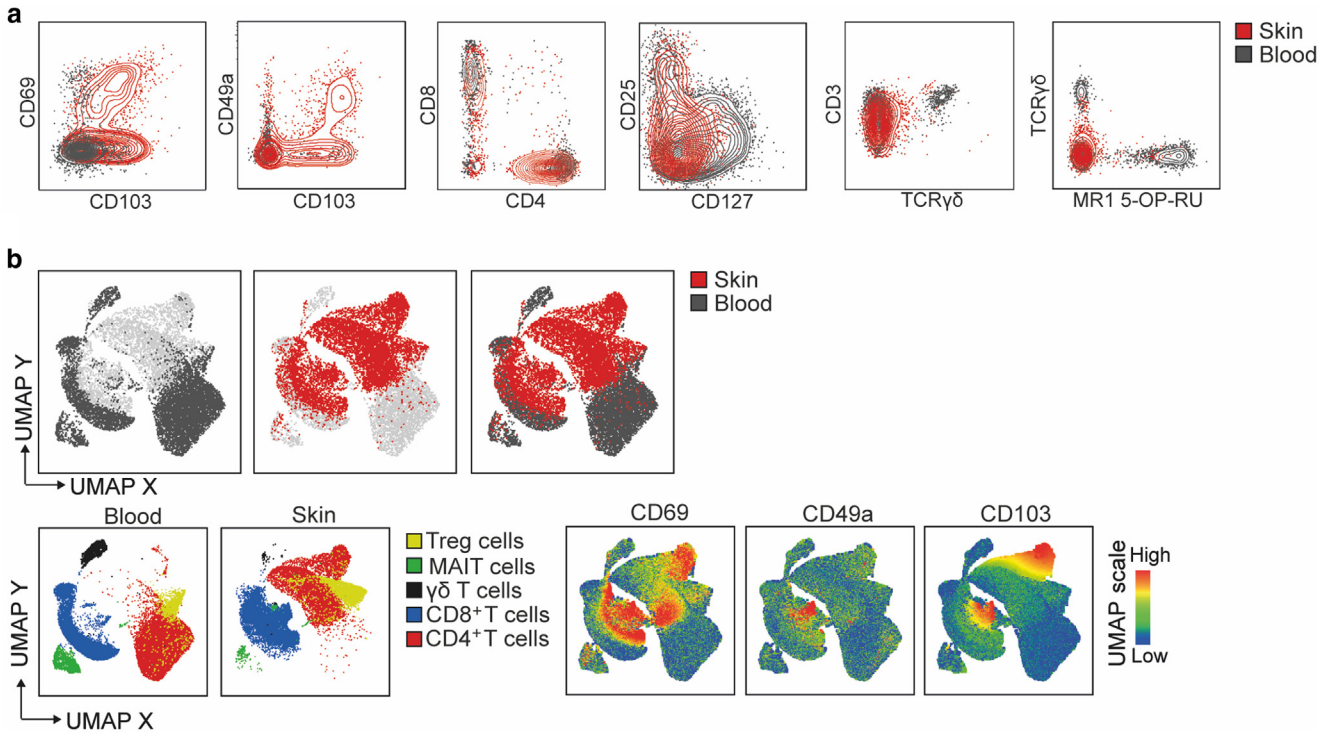

Figure 5. Identification of tissue-resident lymphocytes in healthy skin. (**a**) Overlay plots showing the different representations of respective marker expressions on T cells from peripheral blood (in gray) and skin (in red). (**b**) UMAP plots of total human T cells. Clusters are based on the expression of nine phenotypic markers (CD103, CD69, CD49a, CD4, CD8, CD127, CD25, TCRγδ, and MR1 5-OP-RU), showing cells stratified by their anatomical origin (skin and peripheral blood, upper row). Fractionation of T-cell subsets in UMAP plots into T_{REG} cells, MAIT cells, γδ T cells, and $CD8^+$ and $CD4^+$ T cells in the skin and blood (lower row, left) and distribution of the expressed tissue-residency markers CD69, CD49a, and CD103 on T cells (lower row, right). MAIT, mucosal-associated invariant T; T_{REG}, regulatory T; UMAP, unsupervised uniform manifold approximation and projection analysis.

substantial proportion of all $CD45^+CD14^-$ lymphocytes in the skin and mucosa, whereas $CD19^+$ B cells were represented by only a minor fraction (Figure 7a and b). Owing to low numbers of retrieved B cells, these were not further characterized. In murine skin and mucosa, the composition of $CD4^+$ and $CD8^+$ T cells was comparable with a phenotype indicative of effector memory T (T_{EM}) cells ($CD62^-CD44^+$) in tissues. In contrast, in blood, all the three subtypes, that is, central memory T cells, T_{EM} cells, and naïve T cells, were found. T cells isolated from murine skin and mucosa expressed the tissue-resident markers CD69 and CD103 or coexpressed both. Using high-dimensional UMAP analysis of total murine T cells—clustering on the basis of the expression of eight phenotypic markers (CD8, CD4, Foxp3, CD25, CD62L, CD44, CD69, and CD103) and stratification by their anatomical origin (mucosa, skin, bone marrow, blood)—we could emphasize the similarities between blood and bone marrow and skin and mucosa (Figure 7c), respectively. Similar to human skin, T cells from murine skin and mucosa exhibited a T_{EM} phenotype with predominantly conventional T-cell subsets and a minor population of regulatory T cells expressing CD69 and CD103. In summary and in line with their anatomical location, skin-derived and mucosa-derived T cells display a unique cluster profile, simultaneously coexpressing markers of tissue residence, which is in contrast to that of T cells from blood and bone marrow.

DISCUSSION

The skin is a barrier tissue that is affected by various inflammatory disorders (Egami et al., 2020; Park and Kupper, 2015). Although the skin is densely populated by multiple types of immune cells, blood samples are the easiest to obtain and therefore remain the major sample source for human immunological studies. Nevertheless, circulating immune cells do not necessarily reflect local immune responses in the skin (Szabo et al., 2019). In this study, we sought to establish a protocol that allows a rapid, epitope-sparing, easy-to-use isolation of immune cells from human skin biopsies in a size routinely taken for diagnostic purposes in the clinic. In this study, we report that enzymatic digestion of skin using optimized concentrations of collagenase IV and DNase for 30 minutes results in abundant cell yields for subsequent analysis with flow cytometry and preserves epitopes readily lost during longer tissue digestion periods. The protocol allowed the detection of both various innate and adaptive leukocytes. T cells were the predominant lymphocyte subset in human skin, exhibited a T_{EM} phenotype, and were proven to be functional. In addition, we showed that the protocol can be also applied to murine skin and mucosa. Thus, the optimized rapid protocol is suitable to study immune cells directly ex vivo without the need for long incubation times and thus can be further used for several downstream applications.

Considering the size of regular biopsies received, cellular yield is one important determinant for further analysis.

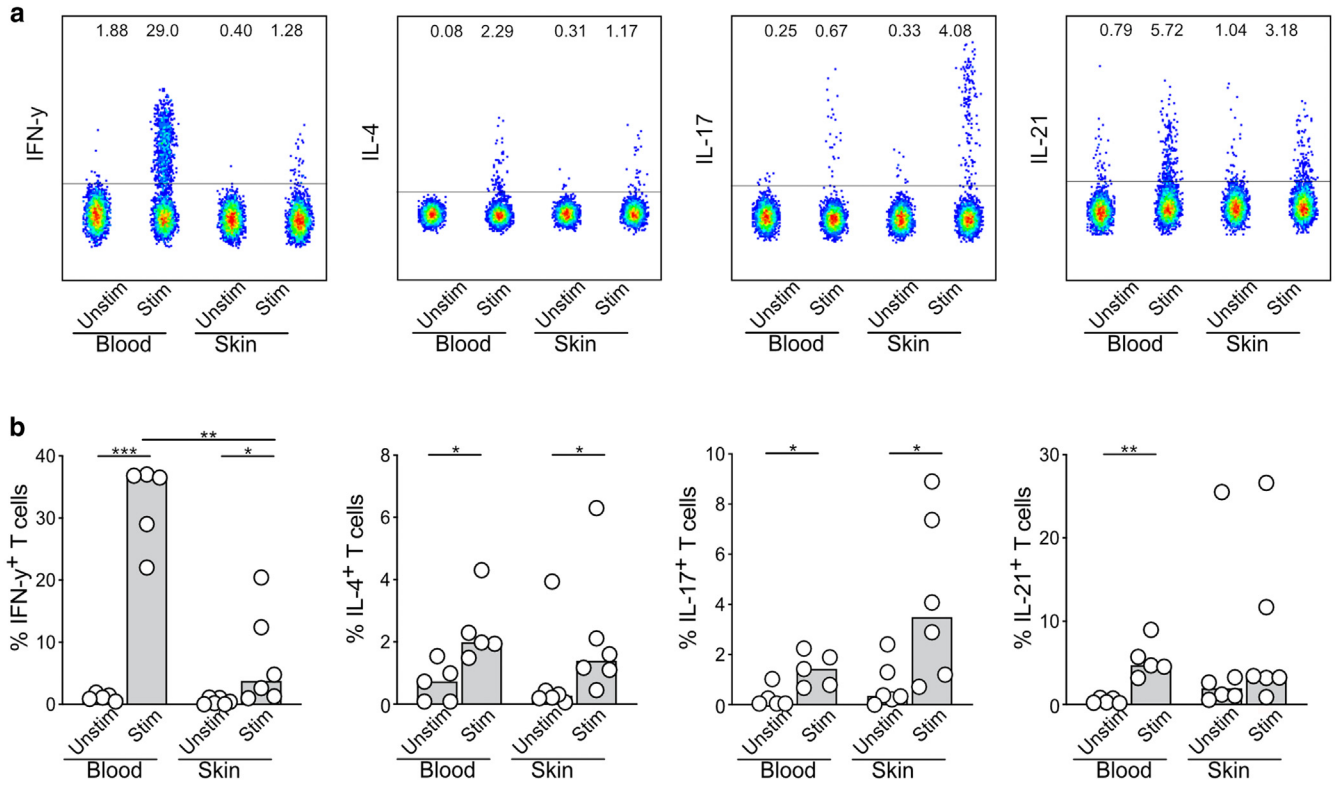

Figure 6. T cells isolated from the skin retain their functional capacity. (**a**) Representative flow cytometry plots showing cytokine production (i.e., IFN-γ, IL-4, IL-17, and IL-21) of blood- and skin-derived T cells on a 4-hour stimulation with PMA/ionomycin. (**b**) Summary of **a** for T cells (median, n = 5–6). Statistical significance was tested using the Wilcoxon signed-rank test or paired *t*-test. $*P < 0.05$, $**P < 0.01$, and $***P < 0.001$. PMA, phorbol 12-myristate-13-acetate; stim, stimulated; unstim, unstimulated.

Moreover, when biopsies are taken, tissue damage may induce immune reactions because nearly all cells in the skin can produce cytokines and chemokines, which in turn impact immune cells in the biopsy even before isolation (Ho and Kupper, 2019). This may be seen by changes in receptor expression that will also be influenced by enzymatic digestion (Du et al., 2021). Furthermore, the research hypothesis needs to be considered. Unlike in our protocol, separating the dermis from the epidermis, as shown by other groups, may be an essential additional step to exclusively study immunological processes in the epidermis (Cheuk et al., 2017, 2014; Sato et al., 2022).

Skin inflammation or injury is accompanied by cellular infiltration of a variety of immune cells (Ho and Kupper, 2019). In humans, T_{RM} cells are the best characterized tissue-resident immune cell subset, which has been shown to permanently reside in various tissues, including the gut, liver, lung, and skin (Oja et al., 2018; Pallett et al., 2020; Sathaliyawala et al., 2013; Strobl et al., 2020; Watanabe et al., 2015; Wong et al., 2016). In addition to T_{RM} cells, skin is also surveilled by infiltrating subsets, such as migratory memory T cells (Watanabe et al., 2015). To assess cellular infiltration by absolute cell counts versus the frequential increase within a given population, we showed that the lost proportion of cells during digestion, filtration, and staining could be estimated with counting beads carried throughout the procedure. T_{RM} cells can be identified using tissue-residency markers. As such, CD69 is upregulated on activation but has been also shown to be expressed by tissue-resident cells, where it opposes the expression of tissue egress receptors (Shiow et al., 2006). CD49a and CD103 are integrins binding to type IV collagen and E-cadherin, respectively, and are therefore important for retention and tissue localization (Szabo et al., 2019). In fact, T cells isolated from healthy human skin using the optimized rapid protocol consisted of conventional $CD4^+$ and $CD8^+$ T cells, with a substantial proportion of these cells expressing tissue-residency markers. Therefore, when T cells isolated from the skin were compared with those from matched peripheral blood, differential clustering of the same cell type was observed. These results are in congruence with those of other studies (Cheuk et al., 2017; Dijkgraaf et al., 2019; Klicznik et al., 2019; Strobl et al., 2020). Unconventional T cells, in particular, mucosal-associated invariant T cells and γδ T cells, were reported to play a role in skin health and in several dermatological diseases (Cai et al., 2011; Cassius et al., 2020; Constantinides et al., 2019; Li et al., 2017; Marshall et al., 2019). However, in healthy skin, we could only detect a minor population of these cell types.

For potential downstream application, we set out to evaluate the functional capacity of T cells isolated from the skin using the optimized rapid protocol. As we have shown with phorbol 12-myristate-13-acetate/ionomycin stimulation and compared with other studies using enzymatic digestion protocols, T cells retained their ability to produce several cytokines, including IL-17, IL-4, and IFNγ, which have been

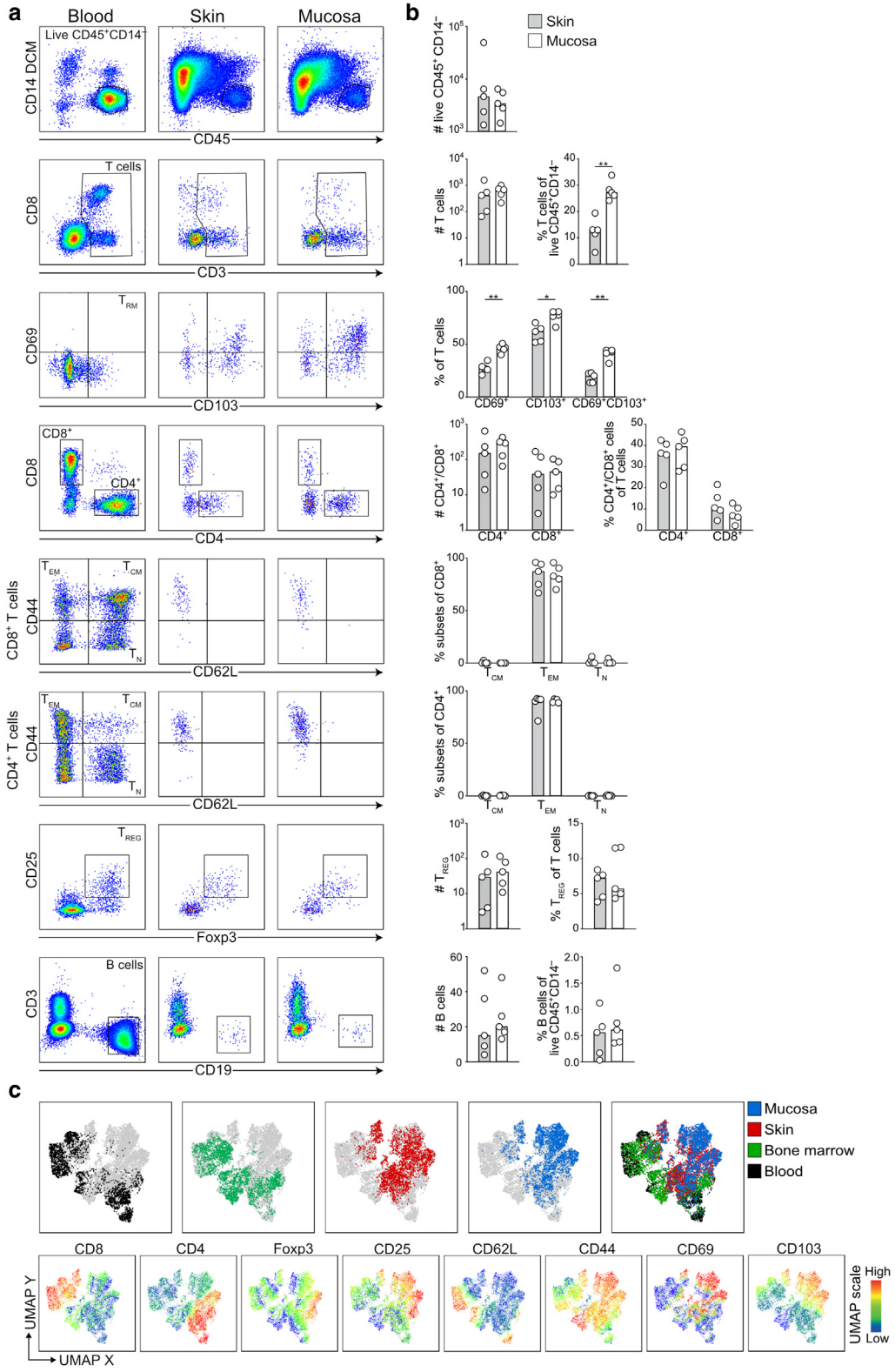

Figure 7. Immune cell retrieval from murine skin and mucosa. (**a**) Representative flow cytometry plots showing the gating strategy to identify respective cell populations in murine blood, skin, and mucosa. (**b**) Summary graphs of **a** for murine skin (in gray) and mucosa (in white) (median, n = 6). Statistical significance was tested using the paired *t*-test. $*P < 0.05$ and $**P < 0.01$. # denotes the number of respective cells. (**c**) UMAP plots of total murine T cells. Clusters are based on the expression of eight markers, showing cells stratified by their anatomical origin (mucosa, skin, bone marrow, and blood; upper row) and the expression of single markers used (lower row, n = 6), respectively. TCM, central memory T; TEM, effector memory T; TN, naive T; UMAP, unsupervised uniform manifold approximation and projection analysis.

shown to play a role in diseases such as psoriasis, atopic dermatitis, and vitiligo, respectively (Cheuk et al., 2017; Du et al., 2021; Jung et al., 2003; Strobl et al., 2020).

Mouse models are commonly used to understand immunopathological mechanisms (Miyagawa et al., 2010). Therefore, in a final set of experiments, we aimed to evaluate the potential applicability of the rapid isolation protocol for tissues from other species, such as mice. Our findings revealed that the isolation protocol can be not only applied to human skin but also applied to mouse skin and mucosal tissues alike. Anticipated numbers of isolated lymphocytes may vary depending on the strain of the mice and the experimental conditions used because we and others have observed a notable variability in the numbers of isolated lymphocytes (Sheridan and Lefrançois, 2012). In line with other reports, we found $CD4^+$ T cells in murine skin and oral mucosa to be the predominant subset (Park et al., 2017), followed by $CD8^+$ T_{RM} cells, which are known to reside almost exclusively in the murine epidermis (Clark et al., 2006a; Gebhardt et al., 2011; Szabo et al., 2019; Watanabe et al., 2015). Phenotypically and in agreement with other reports (Clark, 2010; Tokura et al., 2020), we could confirm a predominant T_{EM} phenotype of T_{RM} cells. Interestingly, cells isolated from murine mucosa and skin clearly mapped separately from cells originating from blood or bone marrow, highlighting the importance of differences in local immunity.

Despite the feasibility and new arisen possibilities created by the optimized rapid protocol, some limitations should be taken into account. The spatial arrangement of the cells is a crucial factor to be considered for understanding the underlying mechanism of cell–cell interaction (Miller et al., 2004; Pascual-Reguant et al., 2021). This is a major limitation of isolation methods, where information about precise location within tissue and spatial orientation of the cells is lacking. Therefore, it is advised that the rapid isolation protocol should be supplemented by other methods such as microscopy. As reported by several groups, isolation of lymphocytes from tissue does not allow all cells to be recovered and may impose a bias against certain subsets (Clark et al., 2006a; Steinert et al., 2015). Therefore, the underestimated absolute numbers of T cells using isolation protocols may be complemented by image-based quantitative immunofluorescence microscopy (Steinert et al., 2015). Moreover, enzymatic digestion of skin may reduce surface molecule expression (Reichard and Asosingh, 2019). For instance, CD56, a marker of NK cells, appears to be a particularly labile molecule because a significant reduction in its expression levels was even observed after both cryopreservation (Kadić et al., 2017) and formalin fixation (Curry et al., 2000). However, we found that most glycoproteins used for the phenotypic characterization of lymphoid populations remained largely unaffected during a 30-minute incubation period.

In this study, we showed that our protocol rapidly isolates lymphocytes from the skin and was gentle in an epitope-preserving manner while still extracting substantial numbers of functional cells, making it a vital step at the beginning of a wide range of research applications. Besides a detailed phenotypic analysis by flow cytometry, skin-derived lymphocytes can be further isolated by FACS to confidently answer specific research questions by minimizing interference from other cell types. These purified cells can be used in a variety of ways in life science research and allow analyses of a single cell type to be performed, including RNA sequencing and epigenetic approaches, both being of particular interest for disease monitoring as well as identification of potential therapeutic targets. The direct application of purified cells for incorporation into tissue models, the use of cells for adoptive cell transfer experiments in different animal models, or the possible increase in sensitivity of analytical methods used in clinical practice (e.g., cell isolation for FISH analyses) may be further options.

In summary, we present a rapid, easy-to-use method for the isolation of immune cells from skin biopsies that can be integrated into clinical research for the identification of potential therapeutic targets or other downstream applications.

MATERIALS AND METHODS

Study material

Blood and skin samples from 34 individuals (4 males, 30 females) were included in this study. The participants had a median age of 57 years (18–91 years). All individuals were seen and operated on at the Department of Gynecology and Obstetrics or the Department of Dermatology and Allergology, University Hospital of Giessen and Marburg in Marburg (Germany). The epidemiological data and the location of sampling are listed in Table 1. The study was approved by the Ethics Committee of the Medical Faculty of the Philipps-Universität Marburg (Az. 169/19), and written informed consent was obtained from all participants. For murine experiments, blood, bone marrow, skin, and mucosa were derived from HLA-DRA1*01:01-DRB1*04:02/-DQA1*03:01, -DQB1*03:02 (DQ8)-transgenic C57Bl/6J mice expressing the human CD4 coreceptor deficient for I-Aβ ($I\text{-}A\beta^{-/-}$). Samples were obtained in parallel to supervised animal experiments approved by the local Laboratory Animal Ethics Committee at the Philipps-Universität Marburg (Marburg, Germany). The experiments were done in compliance with local policies and guidelines on the use of laboratory animals.

Collection and processing of peripheral blood, skin biopsies, and murine tissue

PBMCs were isolated from citrate-phosphate-dextrose-adenine–containing peripheral blood samples by density gradient sedimentation using Lymphocyte Separation Medium (Capricorn Scientific, Ebsdorfergrund, Germany) and subsequently stained for flow cytometry. Healthy adult human skin was collected after elective surgical procedures at the Department of Gynecology and Obstetrics, University Hospital of Giessen and Marburg in Marburg and directly transferred into RPMI 1640 medium (Capricorn Scientific). Specifically, 4-mm punch biopsies were taken from the samples derived from surgical interventions to assure comparability with biopsies routinely taken in the clinic. For comparative experiments and method validation, the protocol was also applied to biopsies of 6 and 8 mm, respectively. Skin biopsies were then manually minced with sterile scalpels into small fragments, followed by enzymatic digestion using collagenase IV (enzymatic activity ≥125 collagen digestion unit/mg solid, 0.5–5.0 FALGPA units/mg solid, Sigma-Aldrich, St. Louis, MO) and DNase I (Roche, Mannheim, Germany) at different concentrations in RPMI 1640 medium for the respective incubation time (as indicated below) at 37 °C. To stop enzymatic digestion, a complete RPMI 1640 medium containing 10% fetal bovine serum (Sigma-Aldrich) was added. After digestion, the homogenized tissue was filtered through a 40-μm cell strainer

(Corning, Sigma-Aldrich) and pushed through with a sterile syringe plunger. To increase cell yield, the filters were flushed twice, and cell-containing tubes were centrifuged to obtain a pellet and washed twice in PBS (Capricorn Scientific), including 2% fetal bovine serum (Sigma-Aldrich) with cells subsequently used for flow cytometry. The optimized rapid digestion protocol was compared with a commercially available whole skin dissociation kit, following the manufacturers' instructions with minor modifications (Miltenyi Biotec, Bergisch Gladbach, Germany). In brief, the punch biopsy was transferred into buffer L containing the appropriate amounts of enzyme P, enzyme D, and enzyme A for a 2-hour tissue digestion at 37 °C in a humidified atmosphere at 5% carbon dioxide. Subsequently, the samples were diluted with a culture medium, followed by tissue disruption using the gentleMacs (Miltenyi Biotec) program h_skin_01. Finally, the samples were filtered, washed, and prepared for analysis with flow cytometry in parallel with the comparative samples as described earlier.

Determination of absolute cell counts

A total of 50 μl of Sphero AccuCount Blank Particles (5.2 μm, Spherotech, Lake Forest, IL), corresponding to 50,400 particles in total, were added to the medium containing the minced skin before enzymatic digestion. Counting beads were retained and were thus followed throughout the sample processing until analysis with flow cytometry. It was assumed that the proportion of beads lost during the process was equal to the proportion of cells lost. The absolute cell count (×) was calculated as follows:

counting beads detected/50,400 (total number of beads added) = number of cells detected/×.

Functional in vitro analysis of isolated skin-derived T cells

Isolated cells from the skin and PBMCs of the respective subjects were plated in round-bottom 96-well plates in a complete RPMI 1640 medium and stimulated with a cell activation cocktail (BioLegend, San Diego, CA) containing phorbol 12-myristate-13-acetate, ionomycin, and brefeldin A according to the manufacturer's instructions for 4 hours at 37 °C and 5% carbon dioxide. Subsequently, the cells were stained for flow cytometry as described below.

Flow cytometry staining and data analysis

For flow cytometry, cells were stained with fluorescently labeled antibodies directly after cell processing. For extracellular staining, samples were incubated for 20 minutes at room temperature. For experiments with human tissues, the following mAbs were used for extracellular staining: CD4-KIRAVIA Blue 520 (SK3), CD3-PerCP-Cy5.5 (SK7), CD45-AF700 (HI30), CXCR3-BV421 (G025H7), CD14-BV510 (MSE2), CD19-BV510 (HIB19), CCR6-BV711 (G034E3), CD19-PerCP-Cy5.5 (HIB19), BDCA2-BV421 (201A), CD161-BV605 (HP3G10), CD127-BV650 (A019DS), CD3-BV785 (SK7), CD1c-PE-Cy7 (L161), CD49a-AF647 (TS2/7), CD69-APC/FireTM750 (FN50), CD127-BV650 (A019D5), CD8-BV785 (SK1), CD103-PE-Dazzle594 (Ber-ACT8), CD16-BV711 (3G8), CD15-AF488 (HI98), CD11c-AF647 (3.9), CD14-APC/FireTM750 (63D3), CD1a-BV605 (HI149), HLA-DR-BV650 (L243), CCR3-PE (5E8), and CD25-PE-Cy7 (M-A251, all from BioLegend) and LIVE/DEAD Fixable Aqua Dead Cell Stain Kit and CD8-QD605 (3B5, both from Invitrogen by Thermo Fisher Scientific, Waltham, MA); NKG2A-FITC (REA110, Miltenyi Biotec); CD56-PE CF594 (CD56, BD Biosciences, San Jose, CA); and TCRγδ-PE-Cy5.5 (Immunotech Beckman Coulter, Marseille, France). The 5-OP-RU MR1 tetramers were developed by J. McCluskey, J. Rossjohn, and D. Fairlie (National Institutes of Health Tetramer Core Facility at Emory University, Atlanta, GA) and were allowed to be distributed with the permission of the University of Melbourne (Melbourne, Australia). For experiments with murine tissues, the following mAbs were used for extracellular staining: CD3-PerCP-Cy5.5 (17A2), CD45-Alexa700 (30-F11), CD69-APC-Cy7 (H1.2F3), CD62L-BV421 (MEL-14), CD44-BV605 (IM7), CD8-BV785 (53-6.7), CD103-PE-DazzleTM 594 (2E7), CD19-BV605 (6D5), and Zombie NIRTM Fixable Viability-APC-Cy7 (all from BioLegend) and CD4-FITC (RM4-5), CD25-PE (PC61.5), and LIVE/DEAD Fixable Aqua Dead Cell Stain Kit (all from Invitrogen by Thermo Fisher Scientific). After extracellular staining and, if performed, before intracellular staining, cells were fixed using fixation/permeabilization buffer (eBioscience FOXP3/Transcription, Invitrogen, San Diego, CA). Cells were stained intracellularly for 20 minutes at 4 °C for functional readouts in permwash buffer (eBioscience FOXP3/Transcription, Invitrogen). For intracellular staining in human tissue experiments, the following mAbs were used: CD68-BV421 (Y1/82A), IL4-BV421 (MP4-25D2), and IFN-γ-BV711 (4S.B3, all from BioLegend) and IL-17-BV650 (N49-653) and IL-21-PE (3A3-N21, both from BD Biosciences). For intracellular staining in murine tissue, the mAb Foxp3-APC (FJK-16s, Invitrogen by Thermo Fisher Scientific) was used. Samples were acquired on the BD FACS LSR Fortessa equipped with four lasers (BD Biosciences). Standard flow cytometry data analysis and UMAP analysis were performed using FlowJo, version 10.8 (BD Biosciences).

Statistical analysis

Statistical analysis was conducted using GraphPad Prism, version 9 (GraphPad Software, San Diego, CA). Normality testing was performed using the D'Agostino–Pearson omnibus normality test. Statistical significance was, for normally distributed data, assessed using paired student *t*-test or repeated measure one-way ANOVA followed by Tukey's multiple comparison test, if samples were paired. For non-normally distributed data, Wilcoxon matched-pairs signed rank test was used for matched pairs of data, or Mann–Whitney test was used when datasets were unmatched. For multiple comparisons, data were analyzed using Friedman test for matched or Kruskal–Wallis for unmatched comparisons followed by Dunn's multiple comparisons test. Differences were considered statistically significant at $*P < 0.05$, $**P < 0.01$, and $***P < 0.001$ or considered not to reach significance.

Protocol

Reagents.

- incomplete RPMI 1640 medium: RPMI 1640 medium without additives (Capricorn Scientific);
- complete RPMI 1640 medium: RPMI 1640 medium supplemented with 100× penicillin/streptomycin with L-Glutamine (Thermo Fisher Scientific) and 10% fetal bovine serum (Sigma-Aldrich);
- Collagenase IV (Sigma-Aldrich); and
- DNase I (Roche)

Equipment.

- feather disposable scalpel (Feather Safety Razor, Köln, Germany);
- Petri dish, Nunclon Delta Surface (Thermo Fisher Scientific);
- a 5 ml test tube with lid, Polystyrene Round-Bottom Tube (Falcon, Corning, Corning, NY);
- PTFE Stirrer Bar, Micro, 5 × 2 mm (Cowie Technology Group, Ridgeway, United Kingdom);
- water Bath/Magnetic Stirrer System RET Basic (IKA Labortechnik, Staufen, Germany);

- a 40-μm cell strainer (Sarstedt, Nümbrecht, Germany);
- Rotina 420R Centrifuge (Hettich Zentrifugen, Tuttlingen, Germany); and
- Nunc 96-Well Polystyrene Conical Bottom MicroWell Plates (Thermo Fisher Scientific)

Procedure. For details, please refer to Figure 1.

1 We added 200 μl of incomplete RPMI 1640 medium into a petri dish and added the skin biopsy.
2 We minced the skin biopsy using two scalpels. We mechanically minced until only small fragments are left. This increases the skin surface area for the subsequent enzymatic digestion.
3 We transferred the tissue into a 5-ml test tube with a lid.
4 We flushed the petri dish with an additional 300 μl of incomplete RPMI 1640 medium and pooled everything. Flushing allows for the recovery of the remaining small fragments and cells after mechanical digestion.
5 We added a cylindrical magnet in a size of 5 × 2 mm and the respective volumes of enzymes so that the final concentration is 1 μg/ml of DNase and 1.7 μg/ml of collagenase IV in the test tube.
6 We put the test tube into a floating rack and let it incubate in a water bath at 37 °C on a magnetic stirrer for 30 minutes. We made sure to avoid temperature fluctuation during incubation, not to influence the rate of enzymatic reaction. The optimum temperature for both enzymes used in this protocol was 37 °C.
7 After 30 minutes, we stopped the enzymatic digestion by adding 2 ml of complete RPMI 1640 medium.
8 We filtered the cells through a 40-μm filter put on a 50-ml Falcon tube and pushed the final pieces of tissue through the filter using, for example, the sterile plunger of a syringe.
9 We flushed the filter by adding 2 ml complete RPMI 1640 medium.
10 We spun the tube at 1,500 r.p.m. for 5 minutes.
11 We discarded the supernatant and resuspend the cells in an appropriate volume depending on the nature and scale of the subsequent experiments. For flow cytometry, we resuspend the cells in a final volume of 200 μl for the subsequent plating of 200 μl per well into a 96 conical-bottom well plate and started staining them for flow cytometry accordingly.

Please note that the following procedure is applicable to skin biopsies with sizes from 4 to 8 mm.

Data availability statement

No large datasets were generated or analyzed during this study. The raw data supporting the conclusion of this article will be made available on request to the corresponding author without undue reservation.

ORCIDs

Alexandra Polakova: http://orcid.org/0000-0002-4792-9306
Christoph Hudemann: http://orcid.org/0000-0001-5807-6882
Felix Wiemers: http://orcid.org/0000-0003-1311-2485
Arturas Kadys: http://orcid.org/0000-0002-7314-8255
Niklas Gremke: http://orcid.org/0000-0002-9015-3646
Manuel Lang: http://orcid.org/0000-0003-3571-5666
Lutz Zwiorek: http://orcid.org/0000-0003-1627-0307
Wolfgang Pfützner: http://orcid.org/0000-0002-8721-724X
Michael Hertl: http://orcid.org/0000-0002-5494-2461
Christian Möbs: http://orcid.org/0000-0002-5197-7669
Christine L. Zimmer: http://orcid.org/0000-0001-7240-6622

CONFLICT OF INTEREST

The authors state no conflict of interest.

ACKNOWLEDGMENTS

We acknowledge the professional assistance of the Center for Human Genetics at Philipps-Universität Marburg (Marburg, Germany). This work was funded by the Deutsche Forschungsgemeinschaft (German Research Foundation, — FOR 2497 Pegasus, subprojects TP2 (PF 344/4-1 to WP and MO 2076/4-2 to CM) and TP8 (HE 1602/16-1 and HE 1602/16-2 to MH) and supported by research grants from the Von Behring-Röntgen-Stiftung (project number 69-0026 to CZ) and the Stiftung P.E. Kempkes (04/2021 to CZ). Open Access funding provided by the Open Acess Publication Fund of Philipps-Universität Marburg with support of the Deutsche Forschungsgemeinschaft (DFG, German Research Foundation). This work was conducted in Marburg, Germany.

AUTHOR CONTRIBUTIONS

Conceptualization: CLZ, AP; Data Curation: CLZ, AP, CM; Formal Analysis: CLZ, AP; Funding Acquisition: CLZ, CM, WP, MH; Investigation: CLZ, AP, CH, ML; Methodology: CLZ, AP, CH; Project Administration: CLZ, CM, WP, MH; Resources: FW, NG, AK, LZ, ML, CH, WP, MH; Supervision: CLZ, CM; Validation: CLZ, AP; Visualization: CLZ, AP; Writing — Original Draft Preparation: CLZ, AP; Writing — Review and Editing: CLZ, AP, CM, CH, WP, MH.

REFERENCES

Alkon N, Bauer WM, Krausgruber T, Goh I, Griss J, Nguyen V, et al. Single-cell analysis reveals innate lymphoid cell lineage infidelity in atopic dermatitis. J Allergy Clin Immunol 2022;149:624–39.

Brüggen MC, Klein I, Greinix H, Bauer W, Kuzmina Z, Rabitsch W, et al. Diverse T-cell responses characterize the different manifestations of cutaneous graft-versus-host disease. Blood 2014;123:290–9.

Cai Y, Shen X, Ding C, Qi C, Li K, Li X, et al. Pivotal role of dermal IL-17-producing γδ T cells in skin inflammation [published correction appears in Immunity 2011;35:649] Immunity 2011;35:596–610.

Cassius C, Branchtein M, Battistella M, Amode R, Lepelletier C, Jachiet M, et al. Persistent deficiency of mucosal-associated invariant T cells during dermatomyositis. Rheumatology (Oxford) 2020;59:2282–6.

Chen L, Shen Z. Tissue-resident memory T cells and their biological characteristics in the recurrence of inflammatory skin disorders. Cell Mol Immunol 2020;17:64–75.

Cheuk S, Schlums H, Gallais Sérézal I, Martini E, Chiang SC, Marquardt N, et al. CD49a expression defines tissue-resident CD8+ T cells poised for cytotoxic function in human skin. Immunity 2017;46:287–300.

Cheuk S, Wikén M, Blomqvist L, Nylén S, Talme T, Ståhle M, et al. Epidermal Th22 and Tc17 cells form a localized disease memory in clinically healed psoriasis. J Immunol 2014;192:3111–20.

Clark RA. Skin-resident T cells: the ups and downs of on site immunity. J Invest Dermatol 2010;130:362–70.

Clark RA, Chong B, Mirchandani N, Brinster NK, Yamanaka K-I, Dowgiert RK, et al. The vast majority of CLA+ T cells are resident in normal skin. J Immunol 2006a;176:4431–9.

Clark RA, Chong BF, Mirchandani N, Yamanaka K-I, Murphy GF, Dowgiert RK, et al. A novel method for the isolation of skin resident T cells from normal and diseased human skin. J Invest Dermatol 2006b;126:1059–70.

Constantinides MG, Link VM, Tamoutounour S, Wong AC, Perez-Chaparro PJ, Han SJ, et al. MAIT cells are imprinted by the microbiota in early life and promote tissue repair. Science 2019;366:eaax6624.

Curry MP, Norris S, Golden-Mason L, Doherty DG, Deignan T, Collins C, et al. Isolation of lymphocytes from normal adult human liver suitable for phenotypic and functional characterization. J Immunol Methods 2000;242:21–31.

Dijkgraaf FE, Matos TR, Hoogenboezem M, Toebes M, Vredevoogd DW, Mertz M, et al. Tissue patrol by resident memory CD8+ T cells in human skin [published correction appears in Nat Immunol 2020;21:696]. Nat Immunol 2019;20:756–64.

Du W, Lenz D, Köhler R, Zhang E, Cendon C, Li J, et al. Rapid Isolation of Functional ex vivo Human Skin Tissue-Resident Memory T lymphocytes. Front Immunol 2021;12:624013.

Egami S, Yamagami J, Amagai M. Autoimmune bullous skin diseases, pemphigus and pemphigoid. J Allergy Clin Immunol 2020;145:1031–47.

Fan X, Rudensky AY. Hallmarks of tissue-resident lymphocytes. Cell 2016;164:1198–211.

Gebhardt T, Whitney PG, Zaid A, Mackay LK, Brooks AG, Heath WR, et al. Different patterns of peripheral migration by memory CD4+ and CD8+ T cells. Nature 2011;477:216–9.

Geissmann F, Manz MG, Jung S, Sieweke MH, Merad M, Ley K. Development of monocytes, macrophages, and dendritic cells [published correction appears in Science 2010;330:1319] Science 2010;327:656–61.

Hashimoto D, Chow A, Noizat C, Teo P, Beasley MB, Leboeuf M, et al. Tissue-resident macrophages self-maintain locally throughout adult life with minimal contribution from circulating monocytes. Immunity 2013;38:792–804.

Ho AW, Kupper TS. T cells and the skin: from protective immunity to inflammatory skin disorders. Nat Rev Immunol 2019;19:490–502.

Hoytema van Konijnenburg DP, Mucida D. Intraepithelial lymphocytes. Curr Biol 2017;27:R737–9.

Jung T, Moessner R, Neumann C. Naïve CD4+ T cells from patients with atopic dermatitis show an aberrant maturation towards IL-4-producing skin-homing CLA+ cells. Exp Dermatol 2003;12:555–62.

Kadić E, Moniz RJ, Huo Y, Chi A, Kariv I. Effect of cryopreservation on delineation of immune cell subpopulations in tumor specimens as determinated by multiparametric single cell mass cytometry analysis. BMC Immunol 2017;18:6.

Klicznik MM, Morawski PA, Höllbacher B, Varkhande SR, Motley SJ, Kuri-Cervantes L, et al. Human CD4+CD103+ cutaneous resident memory T cells are found in the circulation of healthy individuals. Sci Immunol 2019;4. eeav8995.

Kumar BV, Ma W, Miron M, Granot T, Guyer RS, Carpenter DJ, et al. Human tissue-resident memory T cells are defined by core transcriptional and functional signatures in lymphoid and mucosal sites. Cell Rep 2017;20:2921–34.

Li J, Reantragoon R, Kostenko L, Corbett AJ, Varigos G, Carbone FR. The frequency of mucosal-associated invariant T cells is selectively increased in dermatitis herpetiformis. Australas J Dermatol 2017;58:200–4.

Marshall AS, Silva JR, Bannerman CA, Gilron I, Ghasemlou N. Skin-resident γδ T cells exhibit site-specific morphology and activation states. J Immunol Res 2019;2019:9020234.

Miller MJ, Safrina O, Parker I, Cahalan MD. Imaging the single cell dynamics of CD4+ T cell activation by dendritic cells in lymph nodes. J Ex. Med 2004;200:847–56.

Miyagawa F, Gutermuth J, Zhang H, Katz SI. The use of mouse models to better understand mechanisms of autoimmunity and tolerance. J Autoimmun 2010;35:192–8.

Nieto JC, Cantó E, Zamora C, Ortiz MA, Juárez C, Vidal S. Selective loss of chemokine receptor expression on leukocytes after cell isolation. PLoS One 2012;7:e31297.

Oja AE, Piet B, Helbig C, Stark R, van der Zwan D, Blaauwgeers H, et al. Trigger-happy resident memory CD4+ T cells inhabit the human lungs. Mucosal Immunol 2018;11:654–67.

Pallett LJ, Burton AR, Amin OE, Rodriguez-Tajes S, Patel AA, Zakeri N, et al. Longevity and replenishment of human liver-resident memory T cells and mononuclear phagocytes. J Ex. Med 2020;217:e20200050.

Park CO, Kupper TS. The emerging role of resident memory T cells in protective immunity and inflammatory disease. Nat Med 2015;21:688–97.

Park JY, Chung H, Choi Y, Park JH. Phenotype and tissue residency of lymphocytes in the murine oral mucosa. Front Immunol 2017;8:250.

Pascual-Reguant A, Köhler R, Mothes R, Bauherr S, Hernández DC, Uecker R, et al. Multiplexed histology analyses for the phenotypic and spatial characterization of human innate lymphoid cells. Nat Commun 2021;12:1737.

Reichard A, Asosingh K. Best practices for preparing a single cell suspension from solid tissues for flow cytometry. Cytometry A 2019;95:219–26.

Salimi M, Subramaniam S, Selvakumar T, Wang X, Zemenides S, Johnson D, et al. Enhanced isolation of lymphoid cells from human skin. Clin Exp Dermatol 2016;41:552–6.

Sanchez Rodriguez R, Pauli ML, Neuhaus IM, Yu SS, Arron ST, Harris HW, et al. Memory regulatory T cells reside in human skin. J Clin Invest 2014;124:1027–36.

Sathaliyawala T, Kubota M, Yudanin N, Turner D, Camp P, Thome JJC, et al. Distribution and compartmentalization of human circulating and tissue-resident memory T cell subsets. Immunity 2013;38:187–97.

Sato T, Ogawa Y, Ishikawa A, Nagasaka Y, Kinoshita M, Shiokawa I, et al. Revisiting the experimental methods for human skin T-cell analysis. JID Innov 2022;2:100125.

Sheridan BS, Lefrançois L. Isolation of mouse lymphocytes from small intestine tissues. Curr Protoc Immunol 2012. Chapter:Unit3.19.

Shiow LR, Rosen DB, Brdicková N, Xu Y, An J, Lanier LL, et al. CD69 acts downstream of interferon-alpha/beta to inhibit S1P1 and lymphocyte egress from lymphoid organs. Nature 2006;440:540–4.

Simoni Y, Fehlings M, Kløverpris HN, McGovern N, Koo S-L, Loh CY, et al. Human innate lymphoid cell subsets possess tissue-type based heterogeneity in phenotype and frequency [published correction appears in Immunity 2018;48:1060] Immunity 2017;46:148–61.

Steinert EM, Schenkel JM, Fraser KA, Beura LK, Manlove LS, Igyártó BZ, et al. Quantifying memory CD8 T cells reveals regionalization of immunosurveillance. Cell 2015;161:737–49.

Strobl J, Pandey RV, Krausgruber T, Bayer N, Kleissl L, Reininger B, et al. Long-term skin-resident memory T cells proliferate in situ and are involved in human graft-versus-host disease. Sci Transl Med 2020;12. eabb7028.

Szabo PA, Miron M, Farber DL. Location, location, location: tissue resident memory T cells in mice and humans. Sci Immunol 2019;4. eaas9673.

Tokura Y, Phadungsaksawasdi P, Kurihara K, Fujiyama T, Honda T. Pathophysiology of skin resident memory T cells. Front Immunol 2020;11:618897.

Watanabe R, Gehad A, Yang C, Scott LL, Teague JE, Schlapbach C, et al. Human skin is protected by four functionally and phenotypically discrete populations of resident and recirculating memory T cells. Sci Transl Med 2015;7:279ra39.

Wong MT, Ong DEH, Lim FSH, Teng KWW, McGovern N, Narayanan S, et al. A high-dimensional atlas of human T cell diversity reveals tissue-specific trafficking and cytokine signatures. Immunity 2016;45:442–56.

Zou Y, Yuan H, Zhou S, Zhou Y, Zheng J, Zhu H, et al. The pathogenic role of CD4+ tissue-resident memory T cells bearing T follicular helper-like phenotype in pemphigus lesions. J Invest Dermatol 2021;141:2141–50.